第 31 卷第 8 期
2015 年 8 月

无 机 化 学 学 报
CHINESE JOURNAL OF INORGANIC CHEMISTRY

Vol.31 No.8
1609-1618

一系列由柔性 *N*,*N*′-双(3-吡啶甲基)胺构筑的螺旋配合物的合成、结构和性质

岳翠敏　高东昭*　王修光

(天津市功能分子结构与性能重点实验室;无机–有机杂化功能材料化学省部共建教育部重点实验室;
天津师范大学化学学院,天津 300387)

摘要: 合成和表征了 5 个螺旋配位聚合物{[Cu(Hbpma)(H_2O)$_4$]$_2$(SO_4)$_3$·3.5H_2O}$_n$ (**1**)、{[Ni(Hbpma)(H_2O)$_4$]$_4$(SO_4)$_6$·10.75H_2O}$_n$ (**2**)、{[Mn(Hbpma)(H_2O)$_4$](SO_4)$_{1.5}$·3H_2O}$_n$ (**3**)、{[Zn(Hbpma)(H_2O)$_4$]$_4$(SO_4)$_6$·4H_2O·4CH_3OH}$_n$ (**4**)和{[Cu(Hbpma)$_2$(H_2O)$_2$](SO_4)$_2$·9H_2O}$_n$ (**5**),其中 bpma 代表 *N*,*N*′-双(3-吡啶甲基)胺。晶体结构分析表明配合物 **1**~**4** 为一维链状结构,配合物 **5** 为二维层状结构,其中金属离子由质子化的 bpma 配体桥连。值得注意的是,采取反–反式构象的柔性 bpma 配体使得配合物 **1** 和 **2** 为假螺旋链结构,配合物 **3** 和 **4** 为螺旋链结构,配合物 **5** 为螺旋层结构。同时研究了配合物的磁性和热稳定性。

关键词: 金属配合物; *N*,*N*′-双(3-吡啶甲基)胺; 螺旋结构; 磁性; 热稳定性
中图分类号: O614.121; O614.24$^+$1; O614.71$^+$1; O614.81$^+$3　　**文献标识码**: A　　**文章编号**: 1001-4861(2015)08-1609-10
DOI: 10.11862/CJIC.2015.213

Syntheses, Crystal Structures and Properties of a Series of Helical Complexes Constructed by Flexible *N*,*N*′-Bis(3-pyridylmethyl)amine

YUE Cui-Min　GAO Dong-Zhao*　WANG Xiu-Guang

(*Tianjin Key Laboratory of Structure and Performance for Functional Molecules; Key Laboratory of Inorganic-Organic Hybrid Functional Material Chemistry, Ministry of Education; College of Chemistry, Tianjin Normal University, Tianjin* 300387, *China*)

Abstract: Five helical coordination polymers {[Cu(Hbpma)(H_2O)$_4$]$_2$(SO_4)$_3$·3.5H_2O}$_n$ (**1**), {[Ni(Hbpma)(H_2O)$_4$]$_4$(SO_4)$_6$·10.75H_2O}$_n$ (**2**), {[Mn(Hbpma)(H_2O)$_4$](SO_4)$_{1.5}$·3H_2O}$_n$ (**3**), {[Zn(Hbpma)(H_2O)$_4$]$_4$(SO_4)$_6$·4H_2O·4CH_3OH}$_n$ (**4**) and {[Cu(Hbpma)$_2$(H_2O)$_2$](SO_4)$_2$·9H_2O}$_n$ (**5**) (bpma=*N*,*N*′-bis(3-pyridylmethyl)amine) were synthesized and structurally characterized. The single-crystal X-ray analyses indicate that complexes **1**~**4** crystallize in the one-dimensional chain structures and complex **5** shows the two-dimensional layer structure, in which the metal ions are bridged by the protonated bpma ligands. It is noted that the flexible bpma ligands with the *trans-trans* conformation lead to the *pseudo*-helical chains for complexes **1**~**2**, the helical chains for complexes **3**~**4** and a helical layer for complex **5**. The magnetic properties and the thermal behavior are investigated. CCDC: 966929, **1**; 966932, **2**; 966930, **3**; 966931, **4**; 1054736, **5**.

Key words: metal complex; *N*,*N*′-bis(3-pyridylmethyl)amine; helical structure; magnetic property; thermal behavior

收稿日期:2015-04-13。收修改稿日期:2015-05-28。

*通讯联系人。E-mail:tjgaodz@sina.com

0 Introduction

Over the past decades, helical structures have received much attention in coordination chemistry and materials chemistry, because helicity is an essence of life and is also important in advanced materials such as optical devices, enantiomer separation, chiral synthesis, ligand exchange, and selective catalysis[1-3]. One promising approach to construct abiological helices is the use of coordination chemistry to direct the assembly of small component molecules into extended helical polymeric materials[4-5]. The crucial step is the selection of multifunctional organic ligands containing appropriate coordination sites linked by a spacer with specific positional orientation. On the one hand, the ligands should be ditopic and thus capable of bridging metal atoms in certain directions. On the other hand, the ligands should contain steric information that can be interpreted by the arrangement of the bound metal centers, resulting in the formation of helical structures. Up to now, the design of desirable helical structures through the self-assembly of ligands and metal ions has achieved great progress. A great deal of helical coordination polymers, such as one-dimensional helices[6-8], two-dimensional helical layers[9-11], and three-dimensional frameworks containing helical features[12-13], have been systemically investigated in recent years. As the neutral N-donor ligands, 1,3-bis(4-pyridyl)propane (bpp) has proven to be a good candidate for the organization of helices because of its length and flexibility, which can assume different conformations such as TT, TG, GG, and GG′ (considering the relative orientations of the three CH_2 groups, T=*trans*, G=*gauche*)[14-16]. Inspired by the aforementioned considerations, we are interested in exploring various interesting helical structures constructed by another flexible N-donor ligand *N*,*N*′-bis (3-pyridylmethyl)amine (bpma) (the imine group could be protonated) (Scheme 1), which has the similar coordination abilities and conformations with the bpp ligand[17-18]. In this paper, we herein report the crystal structures and properties of five different helical coordination polymers $\{[Cu(Hbpma)(H_2O)_4]_2(SO_4)_3\cdot 3.5H_2O\}_n$ (**1**), $\{[Ni(Hbpma)(H_2O)_4]_4(SO_4)_6\cdot 10.75H_2O\}_n$ (**2**), $\{[Mn(Hbpma)(H_2O)_4](SO_4)_{1.5}\cdot 3H_2O\}_n$ (**3**), $\{[Zn(Hbpma)(H_2O)_4]_2(SO_4)_6\cdot 4H_2O\cdot 4CH_3OH\}_n$ (**4**) and $\{[Cu(Hbpma)_2(H_2O)_2](SO_4)_2\cdot 9H_2O\}_n$ (**5**) bridged by the flexible bpma ligands.

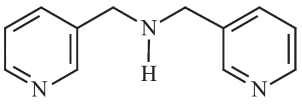

Scheme 1 bpma ligand

1 Experimental

1.1 Material required and instruments

All chemicals were of reagent grade and used without purification. The *N*,*N*′-bis (3-pyridylmethyl) amine (bpma) ligand was prepared using the same method as for *N*,*N*′-bis(2-pyridylmethyl)amine[19]. Elemental analyses for carbon, hydrogen and nitrogen were carried out with a Leeman-Labs CE-440 elemental analyzer. IR spectra were taken with a Nicolet Avatar 370 FT-IR spectrometer in the range of 4 000 ~400 cm^{-1} by KBr pellet technique. The variable temperature magnetic susceptibility measurements were carried out with a Quantum Design MPMS-XL-7 magnetometer in the temperature range 2~300 K at a magnetic field of 1 000 Oe. The molar magnetic susceptibility was corrected from the sample holder and diamagnetic contributions of all constituent atoms by using Pascal′s constants. Thermogravimetric analyses (TGA) were performed on a Perkin-Elmer TGAQ 500 thermogravimetric analyzer under flowing N_2 atmosphere with a heating rate of 5 ℃·min^{-1} up to 650 ℃.

1.2 Preparation of complex $\{[Cu(Hbpma)(H_2O)_4]_2(SO_4)_3\cdot 3.5H_2O\}_n$ (1)

At room temperature, $CuSO_4\cdot 6H_2O$ (26.8 mg, 0.1 mmol) and bpma ligand (19.9 mg, 0.1 mmol) were dissolved in 15 mL distilled water with stirring for 1 h and filtered. After the filtrate was allowed to stand at room temperature for one week, blue block crystals suitable for X-ray structure analysis were grown by slow evaporation. Yield: 38% based on $CuSO_4\cdot 6H_2O$. Anal. Calcd. (%) for $C_{24}H_{51}Cu_2N_6O_{23.50}S_3$: C 28.2; H 5.0; N 8.2; Found(%): C 28.1; H 5.1; N 8.3. IR (KBr disc, cm^{-1}): 3 447(br), 1 437(m), 1 108(m), 814(m), 617(m).

1.3 Preparation of complex {[Ni(Hbpma)(H_2O)$_4$]$_4$(SO_4)$_6$·10.75H_2O}$_n$ (2)

The reaction was carried out following a similar procedure as described for complex **1**, except that $NiSO_4·6H_2O$ was used instead of $CuSO_4·6H_2O$. Light green block crystals were grown by slow evaporation. Yield: 36% based on $NiSO_4·6H_2O$. Anal. Calcd.(%) for $C_{48}H_{109.5}N_{12}Ni_4O_{50.75}S_6$: C 27.5; H 5.2; N 8.0; Found (%): C 27.5; H 5.1; N 8.1. IR (KBr disc, cm^{-1}): 3 222 (br), 1 437(m), 1 079(m), 812(m), 618(m).

1.4 Preparation of complex {[Mn(Hbpma)(H_2O)$_4$](SO_4)$_{1.5}$·3H_2O}$_n$ (3)

The reaction was carried out following a similar procedure as described for complex **1**, except that $MnSO_4·6H_2O$ was used instead of $CuSO_4·6H_2O$. Colorless block crystals were grown by slow evaporation. Yield: 40% based on $MnSO_4·6H_2O$. Anal. Calcd.(%) for $C_{12}H_{28}MnN_3O_{13}S_{1.50}$: C 27.4; H 5.3; N 8.0; Found (%): C 27.3; H 5.4; N 7.9. IR (KBr disc, cm^{-1}): 3 274 (br), 1 436(m), 1 117(m), 811(m), 618(m).

1.5 Preparation of complex {[Zn(Hbpma)(H_2O)$_4$]$_4$(SO_4)$_6$·4H_2O·4CH_3OH}$_n$ (4)

At room temperature, $ZnSO_4·6H_2O$ (26.9 mg, 0.1 mmol) and bpma ligand (19.9 mg, 0.1 mmol) were dissolved in the methanol solution (5 mL methanol and 10 mL distilled water) with stirring for 1 h and filtered. The filtrate was allowed to stand at room temperature for one week, whereupon colorless block crystals suitable for X-ray structure analysis were grown by slow evaporation. Yield: 34% based on $ZnSO_4·6H_2O$. Anal. Calcd.(%) for $C_{52}H_{112}N_{12}O_{48}S_6Zn_4$: C 29.3; H 5.3; N 7.9; Found (%): C 29.4; H 5.3; N 7.8. IR (KBr disc, cm^{-1}): 3 199 (br), 1 438 (m), 1 111(m), 812(m), 618(m).

1.6 Preparation of complex {[Cu(Hbpma)$_2$(H_2O)$_2$](SO_4)$_2$·9H_2O}$_n$ (5)

The reaction was carried out following a similar procedure as described for complex **4**, except that $CuSO_4·6H_2O$ was used instead of $ZnSO_4·6H_2O$. Blue block crystals were grown by slow evaporation. Yield: 31% based on $CuSO_4·6H_2O$. Anal. Calcd.(%) for $C_{24}H_{50}N_6O_{19}S_2Cu$: C 33.7; H 5.9; N 9.8; Found(%): C 33.6; H 6.0; N 9.9. IR (KBr disc, cm^{-1}): 3 435(br), 1 437(m), 1 112(m), 812(m), 618(m).

1.7 Crystallographic data collection and structure determination

The X-ray diffraction measurements of complexes **1**, **4** and **5** were collected with a Bruker CCD area detector diffractometer equipped with a graphite-monochromatic Mo $K\alpha$ radiation source (λ=0.071 073 nm), while those of complexes **2** and **3** were detained with a Bruker APEX-Ⅱ CCD diffractometer. The empirical adsorption corrections by SADABS were carried out[20]. The structures were solved by direct methods using the SHELXS-97 program[21] and refined with SHELXL-97[21] by full-matrix least-squares techniques on F^2. All non-hydrogen atoms were refined anisotropically. All the hydrogen atoms except for some water molecules were generated geometrically and refined isotropically using the riding model. Some free sulfate anions and solvated water molecules are disordered. Crystallographic data and experimental details for structural analyses are summarized in Table 1 and 2. Selected bond lengths and angles are listed in Table 3~7.

CCDC: 966929, **1**; 966932, **2**; 966930, **3**; 966931, **4**; 1054736, **5**.

Table 1　Crystal data and structure refinements for complexes 1 and 2

Complex	1	2
Empirical formula	$C_{24}H_{51}Cu_2N_6O_{23.50}S_3$	$C_{48}H_{109.5}N_{12}Ni_4O_{50.75}S_6$
Formula weight	1 022.97	2 094.17
Crystal system	Monoclinic	Monoclinic
Space group	$P2_1/c$	Pc
a / nm	1.553 26(13)	1.570 13(17)
b / nm	1.637 10(14)	1.647 54(18)
c / nm	1.632 41(14)	2.036 64(16)

Continued Table 1

β / (°)	100.463 0(10)	129.034(5)
V / nm^3	4.081 9(6)	4.092 4(7)
Z	4	2
D_c / (g·cm^{-3})	1.665	1.699
μ / mm^{-1}	1.288	1.172
F(000)	2 124	2 191
Crystal size / mm	0.22×0.15×0.14	0.15×0.14×0.13
θ range / (°)	1.78~25.01	1.24~25.01
Limiting indices (h, k, l)	−18~18, −9~19, −19~19	−18~15, −19~19, −14~24
Reflections collected / unique	20 321 / 7 166 (R_{int}=0.020 2)	20 565 / 10 172 (R_{int}=0.030 2)
Observed reflections	5 758	9 297
Data / restraints / parameters	7 166 / 77 / 560	10 172 / 100 / 1 154
Goodness-of-fit on F^2	1.032	1.048
Final R indices [I>2σ(I)]	R_1=0.040 3, wR_2=0.106 3	R_1=0.043 8, wR_2=0.103 1
R indices (all data)	R_1=0.053 0, wR_2=0.115 6	R_1=0.049 3, wR_2=0.107 8
Largest diff. peak and hole / (e·nm^{-3})	915 and −488	1 440 and −690

Table 2 Crystal data and structure refinements for complexes 3, 4 and 5

Complex	**3**	**4**	**5**
Empirical formula	$C_{12}H_{28}MnN_3O_{13}S_{1.50}$	$C_{52}H_{112}N_{12}O_{48}S_6Zn_4$	$C_{24}H_{50}N_6O_{19}S_2Cu$
Formula weight	525.40	2 127.37	854.36
Crystal system	Monoclinic	Monoclinic	Monoclinic
Space group	$P2_1/n$	$P2_1/n$	$P2_1/c$
a / nm	1.024 51(4)	1.037 1(2)	1.322 94(13)
b / nm	1.694 19(7)	1.690 5(3)	1.303 52(13)
c / nm	1.245 73(6)	1.233 1(2)	2.234 9(2)
β / (°)	90.557 0(10)	90.452(4)	105.585(2)
V / nm^3	2.162 13(16)	2.161 9(7)	3.712 4(6)
Z	4	1	4
D_c / (g·cm^{-3})	1.614	1.634	1.529
μ / mm^{-1}	0.824	1.346	0.785
F(000)	1 096	1 108	1 796
Crystal size / mm	0.12×0.11×0.10	0.15×0.13×0.12	0.14×0.13×0.12
θ range / (°)	2.03~25.01	2.83~25.01	1.60~25.00
Limiting indices (h, k, l)	−10~12, −18~20, −14~14	−12~12, −19~20, −14~9	−10~15, −15~14, −26~22
Reflections collected / unique	10 869 / 3 805 (R_{int}=0.022 3)	10 931 / 3 799 (R_{int}=0.023 4)	18 601 / 6 540 (R_{int}=0.088 0)
Observed reflections	3 333	3 121	3 439
Data / restraints / parameters	3 805 / 57 / 353	3 799 / 61 / 339	6 540 / 38 / 483
Goodness-of-fit on F^2	1.050	1.021	1.000
Final R indices [I>2σ(I)]	R_1=0.032 9, wR_2=0.080 9	R_1=0.031 7, wR_2=0.073 7	R_1=0.052 6, wR_2=0.110 7
R indices (all data)	R_1=0.038 7, wR_2=0.085 1	R_1=0.042 9, wR_2=0.079 6	R_1=0.135 0, wR_2=0.145 7
Largest diff. peak and hole / (e·nm^{-3})	521 and −425	650 and −360	560 and −520

Table 3 Selected bond lengths (nm) and angles (°) for complex 1

Cu(1)-O(14)	0.201 0(2)	Cu(1)-O(16)	0.202 2(2)	Cu(1)-N(2)	0.202 4(3)
Cu(1)-N(4)^i	0.203 4(3)	Cu(1)-O(15)	0.232 3(3)	Cu(1)-O(13)	0.234 5(3)

Continued Table 2

Cu(2)-O(19)	0.199 4(3)	Cu(2)-N(3)	0.202 8(3)	Cu(2)-N(1)	0.203 0(3)
Cu(2)-O(17)	0.203 5(3)	Cu(2)-O(20)	0.227 45(8)	Cu(2)-O(18)	0.247 6(3)
O(14)-Cu(1)-O(16)	175.74(10)	O(14)-Cu(1)-N(2)	86.87(11)	O(16)-Cu(1)-N(2)	94.19(11)
O(14)-Cu(1)-N(4)^{i}	89.86(10)	O(16)-Cu(1)-N(4)^{i}	89.25(11)	N(2)-Cu(1)-N(4)^{i}	175.93(11)
O(14)-Cu(1)-O(15)	87.91(10)	O(16)-Cu(1)-O(15)	87.92(10)	N(2)-Cu(1)-O(15)	92.43(11)
N(4)^{i}-Cu(1)-O(15)	89.87(11)	O(14)-Cu(1)-O(13)	89.81(10)	O(16)-Cu(1)-O(13)	94.32(10)
N(2)-Cu(1)-O(13)	89.23(11)	N(4)^{i}-Cu(1)-O(13)	88.34(11)	O(15)-Cu(1)-O(13)	177.11(9)
O(19)-Cu(2)-N(3)	88.92(12)	O(19)-Cu(2)-N(1)	88.24(12)	N(3)-Cu(2)-N(1)	175.86(12)
O(19)-Cu(2)-O(17)	172.94(11)	N(3)-Cu(2)-O(17)	93.28(12)	N(1)-Cu(2)-O(17)	89.20(12)
O(19)-Cu(2)-O(20)	97.71(10)	N(3)-Cu(2)-O(20)	91.71(11)	N(1)-Cu(2)-O(20)	91.64(11)
O(17)-Cu(2)-O(20)	88.94(11)	O(19)-Cu(2)-O(18)	94.43(11)	N(3)-Cu(2)-O(18)	85.67(11)
N(1)-Cu(2)-O(18)	91.56(11)	O(17)-Cu(2)-O(18)	79.05(11)	O(20)-Cu(2)-O(18)	167.53(9)

Symmetry transformations used to generate equivalent atoms: ^{i} *x*−1, *y*, *z*+1

Table 4　Selected bond lengths (nm) and angles (°) for complex 2

Ni(1)-O(27)	0.198 8(6)	Ni(1)-O(26)	0.205 2(5)	Ni(1)-O(25)	0.205 6(6)
Ni(1)-O(28)	0.206 4(5)	Ni(1)-N(1)	0.209 3(6)	Ni(1)-N(6)^{i}	0.212 9(6)
Ni(2)-O(29)	0.203 7(5)	Ni(2)-O(32)	0.205 2(6)	Ni(2)-O(31)	0.204 6(6)
Ni(2)-O(30)	0.208 1(6)	Ni(2)-N(3)	0.210 3(7)	Ni(2)-N(4)	0.210 3(7)
Ni(3)-O(33)	0.204 5(5)	Ni(3)-O(35)	0.206 3(5)	Ni(3)-O(34)	0.207 1(6)
Ni(3)-O(36)	0.206 9(6)	Ni(3)-N(10)	0.211 2(7)	Ni(3)-N(12)^{iii}	0.211 1(6)
Ni(4)-O(38)	0.203 7(6)	Ni(4)-O(37)	0.206 2(5)	Ni(4)-O(40)	0.207 3(5)
Ni(4)-O(39)	0.209 9(5)	Ni(4)-N(9)^{iii}	0.209 6(7)	Ni(4)-N(7)	0.209 2(7)
O(27)-Ni(1)-O(26)	89.5(2)	O(27)-Ni(1)-O(25)	179.2(3)	O(26)-Ni(1)-O(25)	89.9(2)
O(27)-Ni(1)-O(28)	92.0(2)	O(26)-Ni(1)-O(28)	178.0(2)	O(25)-Ni(1)-O(28)	88.5(2)
O(27)-Ni(1)-N(1)	88.5(3)	O(26)-Ni(1)-N(1)	89.6(2)	O(25)-Ni(1)-N(1)	92.0(2)
O(28)-Ni(1)-N(1)	89.2(2)	O(27)-Ni(1)-N(6)^{i}	88.3(3)	O(26)-Ni(1)-N(6)^{i}	90.5(2)
O(25)-Ni(1)-N(6)^{i}	91.2(2)	O(28)-Ni(1)-N(6)^{i}	90.7(2)	N(1)-Ni(1)-N(6)^{i}	176.8(3)
O(29)-Ni(2)-O(32)	93.6(3)	O(29)-Ni(2)-O(31)	178.3(3)	O(32)-Ni(2)-O(31)	84.9(3)
O(29)-Ni(2)-O(30)	92.1(2)	O(32)-Ni(2)-O(30)	174.2(3)	O(31)-Ni(2)-O(30)	89.4(2)
O(29)-Ni(2)-N(3)	86.2(2)	O(32)-Ni(2)-N(3)	89.4(2)	O(31)-Ni(2)-N(3)	93.0(2)
O(30)-Ni(2)-N(3)	91.8(2)	O(29)-Ni(2)-N(4)	92.6(2)	O(32)-Ni(2)-N(4)	89.5(3)
O(31)-Ni(2)-N(4)	88.2(2)	O(30)-Ni(2)-N(4)	89.3(2)	N(3)-Ni(2)-N(4)	178.3(3)
O(33)-Ni(3)-O(35)	176.2(2)	O(33)-Ni(3)-O(34)	90.5(2)	O(35)-Ni(3)-O(34)	86.0(2)
O(33)-Ni(3)-O(36)	96.7(2)	O(35)-Ni(3)-O(36)	86.9(2)	O(34)-Ni(3)-O(36)	172.8(2)
O(33)-Ni(3)-N(10)	90.6(2)	O(35)-Ni(3)-N(10)	88.1(2)	O(34)-Ni(3)-N(10)	91.8(3)
O(36)-Ni(3)-N(10)	88.5(3)	O(33)-Ni(3)-N(12)^{ii}	87.1(2)	O(35)-Ni(3)-N(12)^{ii}	94.3(2)
O(34)-Ni(3)-N(12)^{ii}	89.3(3)	O(36)-Ni(3)-N(12)^{ii}	90.8(2)	N(10)-Ni(3)-N(12)^{ii}	177.5(3)
O(38)-Ni(4)-O(37)	86.9(2)	O(38)-Ni(4)-O(40)	174.7(2)	O(37)-Ni(4)-O(40)	88.2(2)
O(38)-Ni(4)-O(39)	88.3(2)	O(37)-Ni(4)-O(39)	175.2(2)	O(40)-Ni(4)-O(39)	96.6(2)
O(38)-Ni(4)-N(9)^{iii}	90.5(3)	O(37)-Ni(4)-N(9)^{iii}	91.5(2)	O(40)-Ni(4)-N(9)^{iii}	87.5(2)
O(39)-Ni(4)-N(9)^{iii}	88.8(2)	O(38)-Ni(4)-N(7)	89.8(2)	O(37)-Ni(4)-N(7)	91.6(2)
O(40)-Ni(4)-N(7)	92.4(2)	O(39)-Ni(4)-N(7)	88.1(2)	N(9)^{iii}-Ni(4)-N(7)	176.9(3)

Symmetry transformations used to generate equivalent atoms: ^{i} *x*+2, *y*, *z*+1; ^{ii} *x*+1, −*y*+1, *z*+1/2; ^{iii} *x*+1, −*y*+2, *z*+1/2

Table 5 Selected bond lengths (nm) and angles (°) for complex 3

Mn(1)-O(11)	0.214 55(16)	Mn(1)-O(10)	0.215 71(17)	Mn(1)-O(9)	0.216 15(17)
Mn(1)-O(12)	0.217 51(17)	Mn(1)-N(3)^{i}	0.227 5(2)	Mn(1)-N(1)	0.229 66(19)
O(11)-Mn(1)-O(10)	91.04(7)	O(11)-Mn(1)-O(9)	172.36(7)	O(10)-Mn(1)-O(9)	82.61(7)
O(11)-Mn(1)-O(12)	98.63(6)	O(10)-Mn(1)-O(12)	170.31(6)	O(9)-Mn(1)-O(12)	87.70(7)
O(11)-Mn(1)-N(3)^{i}	90.40(7)	O(10)-Mn(1)-N(3)^{i}	94.26(7)	O(9)-Mn(1)-N(3A)^{i}	85.88(7)
O(12)-Mn(1)-N(3)^{i}	85.01(7)	O(11)-Mn(1)-N(1)	90.88(7)	O(10)-Mn(1)-N(1)	94.38(7)
O(9)-Mn(1)-N(1)	93.81(7)	O(12)-Mn(1)-N(1)	86.23(7)	N(3)i-Mn(1)-N(1)	171.24(7)

Symmetry transformations used to generate equivalent atoms: ^{i} x, y, $z-1$

Table 6 Selected bond lengths (nm) and angles (°) for complex 4

Zn(1)-O(9)	0.207 64(18)	Zn(1)-O(12)	0.208 7(2)	Zn(1)-O(11)	0.210 1(2)
Zn(1)-O(10)	0.212 71(19)	Zn(1)-N(1)	0.217 6(2)	Zn(1)-N(3)^{i}	0.218 7(2)
O(9)-Zn(1)-O(12)	172.48(8)	O(9)-Zn(1)-O(11)	89.90(8)	O(12)-Zn(1)-O(11)	83.99(9)
O(9)-Zn(1)-O(10)	97.69(8)	O(12)-Zn(1)-O(10)	88.48(8)	O(11)-Zn(1)-O(10)	172.39(8)
O(9)-Zn(1)-N(1)	89.42(8)	O(12)-Zn(1)-N(1)	86.69(8)	O(11)-Zn(1)-N(1)	94.43(9)
O(10)-Zn(1)-N(1)	86.22(8)	O(9)-Zn(1)-N(3)^{i}	90.90(8)	O(12)-Zn(1)-N(3)^{i}	93.79(8)
O(11)-Zn(1)-N(3)^{i}	92.98(9)	O(10)-Zn(1)-N(3)^{i}	86.39(8)	N(1)-Zn(1)-N(3)^{i}	172.58(9)

Symmetry transformations used to generate equivalent atoms: ^{i} x, y, $z+1$

Table 7 Selected bond lengths (nm) and angles (°) for complex 5

Cu(1)-N(6)^{i}	0.202 1(4)	Cu(1)-N(1)	0.202 1(4)	Cu(1)-N(3)^{ii}	0.202 9(4)
Cu(1)-N(4)	0.203 6(4)	Cu(1)-O(14)	0.243 5(4)	Cu(1)-O(9)	0.248 6(4)
N(6)^{i}-Cu(1)-N(1)	176.88(17)	N(6)^{i}-Cu(1)-N(3)^{ii}	90.66(16)	N(1)-Cu(1)-N(3)^{ii}	89.94(16)
N(6)^{i}-Cu(1)-N(4)	88.45(16)	N(1)-Cu(1)-N(4)	91.17(16)	N(3)^{ii}-Cu(1)-N(4)	176.02(17)
N(6)^{i}-Cu(1)-O(14)	92.07(14)	N(1)-Cu(1)-O(14)	90.99(14)	N(3)^{ii}-Cu(1)-O(14)	89.56(15)
N(4)-Cu(1)-O(14)	86.61(14)	N(6)^{i}-Cu(1)-O(9)	88.45(14)	N(1)-Cu(1)-O(9)	88.49(14)
N(3)^{ii}-Cu(1)-O(9)	89.80(15)	N(4)-Cu(1)-O(9)	94.05(14)	O(14)-Cu(1)-O(9)	179.18(13)

Symmetry transformations used to generate equivalent atoms: ^{i} $-x+1$, $y-1/2$, $-z+3/2$; ^{ii} $-x+2$, $y-1/2$, $-z+3/2$

2 Results and discussion

2.1 Crystal structures of complexes 1 and 2

The X-ray crystal structure analyses reveal that complexes $\{[Cu(Hbpma)(H_2O)_4]_2(SO_4)_3\cdot 3.5H_2O\}_n$ (**1**) and $\{[Ni(Hbpma)(H_2O)_4]_4(SO_4)_6\cdot 10.75H_2O\}_n$ (**2**) are composed of one-dimensional chains bridged by flexible bpma ligands, free sulfate anions and solvated water molecules. In the coordination environments as depicted in Fig.1 and Fig.S1, there are crystallographically two unique Cu(Ⅱ) centers for complex **1** and four unique Ni(Ⅱ) centers for complex **2** in the asymmetric units, which result in one independent chain for complex **1** and three independent chains for complex **2**. In two complexes, all metal ions display the same six-coordinated distorted octahedral coordination geometries with only different bond lengths and angles coordinated by four water oxygen atoms and two pyridine nitrogen atoms of two different bpma ligands. The M-

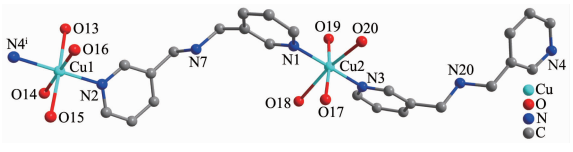

Hydrogen atoms, free sulfate anions and lattice water molecules are omitted for clarity; symmetry code: ^{i} $x-1$, y, $z+1$

Fig.1 View of the coordination environment of the Cu(Ⅱ) centers in complex **1** with limited numbering scheme

O bond distances fall in the range of 0.198 8(6)~0.247 6(3) nm, while the M-N bond lengths vary from 0.202 4(3) to 0.212 9(6) nm, respectively. Meanwhile, the imine groups of bpma ligands are all protonated adopting the *trans-trans* conformation and each bpma ligand bridges two metal ions into a one-dimensional chain structure as shown in Fig.2 and Fig.S2. It should be noted that all bpma ligands spiral around the axis composed of the metal ions, thus the one-dimensional chain should be described as a *pseudo*-helical structure. Along the chains, the intrachain distances between the successive metal ions fall in the range of 1.207 98(10)~1.241 3(1) nm similar to the literature results[22]. The packing of complexes **1** and **2** gives the similar 3D supramolecular framework and the sulfate anions occupy the voids between the 1D chains as shown in Fig.3.

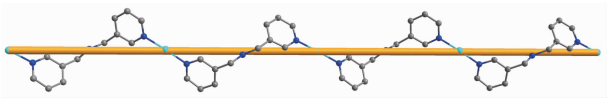

Coordinated water ligands are omitted for clarity

Fig.2　A perspective view of the one-dimensional *pseudo*-helical chain structure in complex **1**

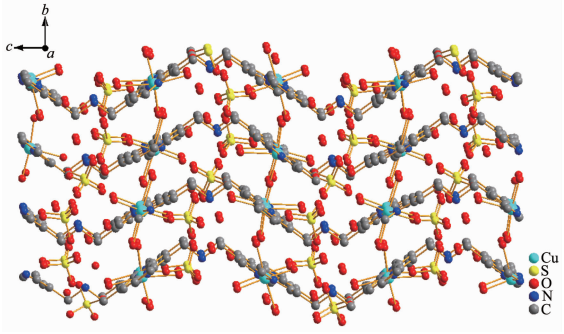

Sulfate anions occupy the voids between the 1D chains

Fig.3　View of the 3D supramolecular framework of complex **1**

2.2　Crystal structures of complexes 3 and 4

Complexes $\{[Mn(Hbpma)(H_2O)_4](SO_4)_{1.5}\cdot 3H_2O\}_n$ (**3**) and $\{[Zn(Hbpma)(H_2O)_4]_4(SO_4)_6\cdot 4H_2O\cdot 4CH_3OH\}_n$ (**4**) also consists of one-dimensional chains bridged by flexible bpma ligands, free sulfate anions and solvated molecules. In the coordination environments as depicted in Fig.4 and Fig.S3, there are crystallographically only one unique Mn(Ⅱ) and Zn(Ⅱ) center in the asymmetric units. In two complexes, the metal ions display the same six-coordinated distorted octahedral coordination geometries with only different bond lengths and angles provided by four water oxygen atoms and two pyridine nitrogen atoms of two different bpma ligands. The M-O bond distances fall in the range of 0.207 64(18)~0.217 51(17) nm, while the M-N bond lengths vary from 0.217 6(2) to 0.229 66(19) nm, respectively. Furthermore, the imine groups of bpma ligands are all protonated assuming the *trans-trans* conformation and each bpma ligand bridges two metal ions into a one-dimensional chain structure as shown in Fig.5 and Fig.S4. It is noteworthy that both the bpma ligands and the metal ions spiral around a 2_1-axis, thus the one-dimensional chain should be described as a single-stranded helical structure. Along the helical chains, the helical pitchs are 1.245 73(6) nm for complex **3** and 1.233 09 (24) nm for complex **4** corresponding to the *c* axis.

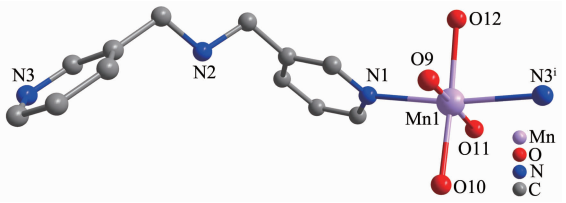

Hydrogen atoms, free sulfate anions and lattice water molecules are omitted for clarity; symmetry code: ⁱ *x*, *y*, *z*−1

Fig.4　View of the coordination environment of the Mn(Ⅱ) center in complex **3** with limited numbering scheme

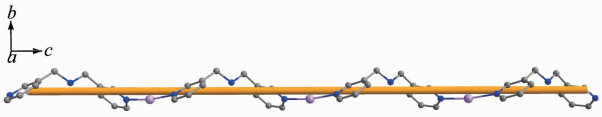

Coordinated water ligands are omitted for clarity

Fig.5　A perspective view of the one-dimensional helical chain structure along the *c* axis in complex **3**

2.3　Crystal structure of complex 5

The X-ray crystal structure analyses reveal that complex $\{[Cu(Hbpma)_2(H_2O)_2](SO_4)_2\cdot 9H_2O\}_n$ (**5**) is composed of two-dimensional layers bridged by flexible bpma ligands, free sulfate anions and lattice water molecules. In the coordination environment as shown in Fig.6, there is crystallographically one

independent Cu(Ⅱ) center in a distorted six-coordinated octahedral geometry. Four nitrogen atoms from four different protonated bpma ligands form the equatorial plane of the Cu(Ⅱ) ion, while two water ligands occupy the apical positions. In the complex, the Cu-N bond distances vary from 0.202 1(4) to 0.203 6(4) nm and the Cu-O bond lengths are 0.243 5(4) and 0.248 6(4) nm, respectively. Meantime, each bpma ligand binds two Cu(Ⅱ) ions leading to a two-dimensional layer as illustrated in Fig.7. It is noteworthy that the bpma ligands in the *trans-trans* conformation form the polymeric helical chains propagating along the crystallographic *b* axis with a helical pitch of 1.303 52(13) nm. Therefore, the 2D sheet can be described as an achiral helical tubular layer in which the left and right helical chains appear alternatively as shown in Fig.7.

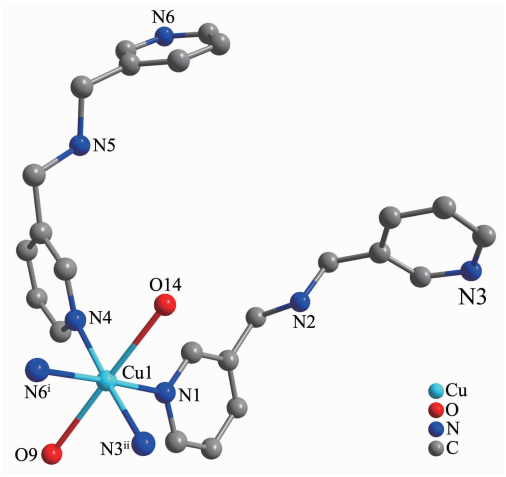

Hydrogen atoms, free sulfate anions and lattice water molecules are omitted for clarity; symmetry code: [i] $-x+1, y-1/2, -z+3/2$; [ii] $-x+2, y-1/2, -z+3/2$

Fig.6 View of the coordination environment of the Cu(Ⅱ) center in complex **5** with limited numbering scheme

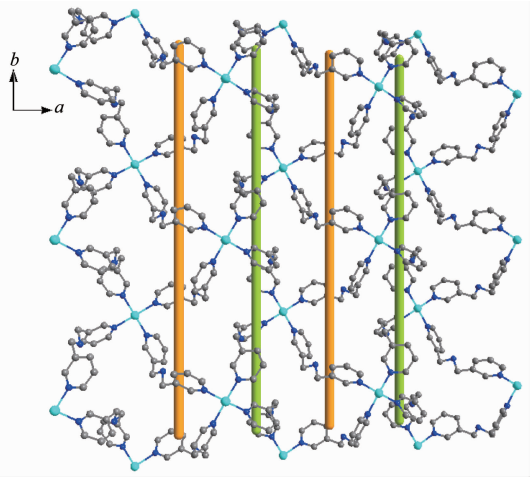

Coordinated water ligands are omitted for clarity

Fig.7 A perspective view of the two-dimensional helical layer structure parallel to the *ab* plane in complex **5**

2.4 Magnetic properties

The variable temperature magnetic susceptibilities of complexes **1**, **3** and **5** were measured and plots of $\chi_M T$ and χ_M^{-1} versus T are shown in Fig.8~10, where χ_M is the magnetic susceptibility per $[Cu(Hbpma)(H_2O)_4]_2(SO_4)_3 \cdot 3.5H_2O$ unit for complex **1**, per $[Mn(Hbpma)(H_2O)_4](SO_4)_{1.5} \cdot 3H_2O$ unit for complex **3** and per $[Cu(Hbpma)_2(H_2O)_2](SO_4)_2 \cdot 9H_2O$ unit for complex **5**. For complex **1**, the $\chi_M T$ value at room temperature is 0.740 $cm^3 \cdot K \cdot mol^{-1}$, which is a little lower than the spin-only value (0.750 $cm^3 \cdot K \cdot mol^{-1}$) expected for two uncorrelated Cu(Ⅱ) centers (S=1/2). For complex **3**, the $\chi_M T$ value at room temperature is 4.310 $cm^3 \cdot K \cdot mol^{-1}$, which is a little lower than the spin-only value (4.375 $cm^3 \cdot K \cdot mol^{-1}$) expected for one high-spin Mn(Ⅱ) center (S=5/2). For complex **5**, the $\chi_M T$ value at room temperature is 0.379 $cm^3 \cdot K \cdot mol^{-1}$, which is close to the spin-only value (0.375 $cm^3 \cdot K \cdot mol^{-1}$) expected for one uncorrelated Cu(Ⅱ) center (S=1/2). On lowering the temperature, the $\chi_M T$ values of three complexes decrease continuously, reaching 0.168 $cm^3 \cdot K \cdot mol^{-1}$ for complex **1**, 4.088 $cm^3 \cdot K \cdot mol^{-1}$ for complex **3** and 0.026 $cm^3 \cdot K \cdot mol^{-1}$ for complex **5** at 2 K. From the plots of χ_M^{-1} against T, the curves of three complexes follow the Curie-Weiss law $\chi_M = C/(T-\theta)$, with fitted

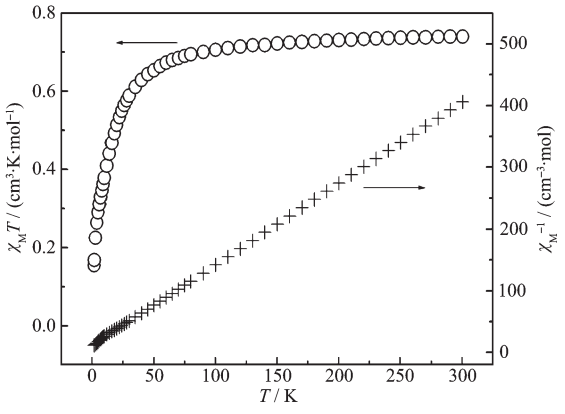

Fig.8 Plots of $\chi_M T$ (○) and χ_M^{-1} (+) versus T for complex **1**

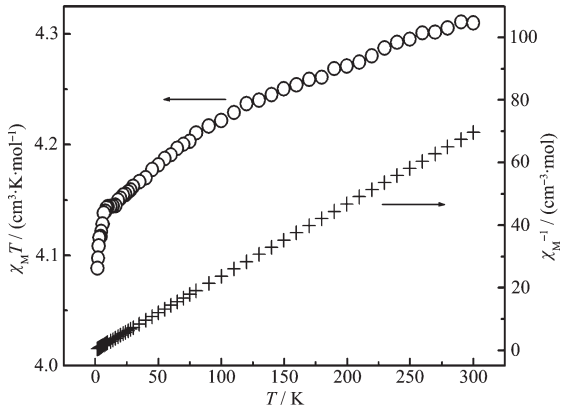

Fig.9　Plots of $\chi_M T$ (○) and χ_M^{-1} (+) versus T for complex **3**

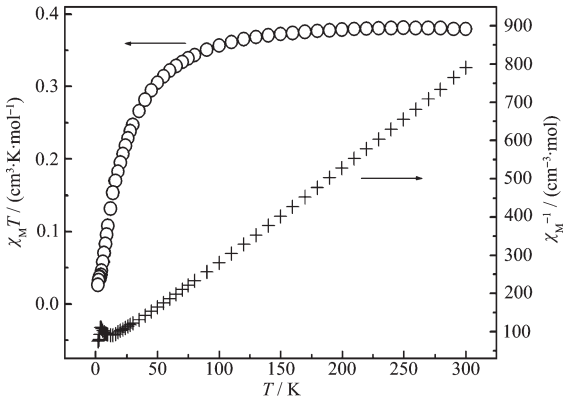

Fig.10　Plots of $\chi_M T$ (○) and χ_M^{-1} (+) versus T for complex **5**

parameters θ=−8.70 K and C=0.76 cm^3·K·mol^{-1} for complex **1**, θ=−0.92 K and C=4.30 cm^3·K·mol^{-1} for complex **3** and θ=−25.53 K and C=0.42 cm^3·K·mol^{-1} for complex **5**, indicating that antiferromagnetic exchange interactions are predominant in three cases. In the crystal structures, the distances between two adjacent Cu(Ⅱ) or Mn(Ⅱ) centers are over 1.1 nm mediated by bpma bridges, so there should be weak antiferromagnetic interactions in three complexes.

2.5　Thermal behavior

All the synthesized complexes are air stable. Thermogravimetric analysis (TGA) was carried out in the interest of studying the thermal stability of these helical structure materials and the TGA curves are provided in Fig.11. The weight loss curves of five complexes are found to be similar exhibiting a two-step weight loss process. The first step of weight loss in the range of 20~200 ℃ should be corresponding to the partly loss of the free or coordinated water molecules. At about 200 ℃, five complexes show the weight loss of 7.02% to 19.66%, less than the calculated values (12.02% to 23.98%). Over the range of 200~500 ℃, the sharp weight loss may be due to the decomposition of the complexes.

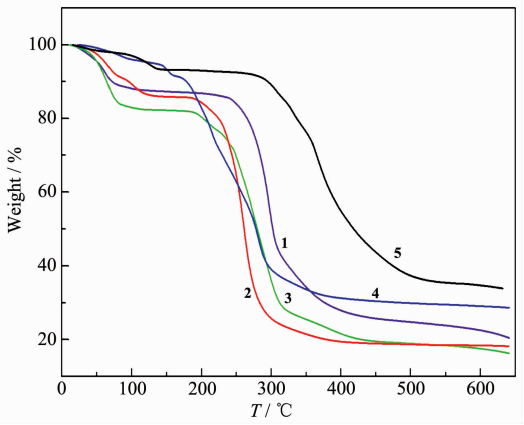

Fig.11　TGA curves for complexes **1**~**5**

3　Conclusions

In summary, five helical structure complexes constructed by flexible bpma ligands were synthesized and structurally characterized in which all protonated bpma ligands assume the *trans-trans* conformation. Complexes **1** and **2** show the *pseudo*-helical chain structures and complexes **3** and **4** exhibit the single-stranded helical chain structures, whereas complex **5** has an achiral helical tubular layer network. These results are beneficial to form more novel helical structures.

Supporting information is available at http://www.wjhxxb.cn

References:

[1] Leong W L, Vittal J J. *Chem. Rev.*, **2011**,**111**:688-764

[2] Li C P, Guo J, Du M. *Inorg. Chem. Commun.*, **2013**,**38**:70-73

[3] Chamayou A C, Makhloufi G, Nafie L A, et al. *Inorg. Chem.*, **2015**,**54**:2193-2203

[4] Lin M J, Jouaiti A, Kyritsakas N, et al. *Chem. Commun.*, **2010**, **46**:115-117

[5] He J H, Chen H Y, Xiao D R, et al. *CrystEngComm*, **2011**, **13**:4841-4845

[6] Xiao D R, Li Y G, Wang E B, et al. *Inorg. Chem.*, **2007**,**46**: 4158-4166

[7] Xin R, Yu X Y, Gao W P, et al. *Inorg. Chem. Commun.*,

2013,**35**:38-41

[8] SONG Shuang(宋爽), CHA Yu-E(查玉娥), WANG Yu-Feng(王育丰), et al. *Chinese J. Inorg. Chem.*(无机化学学报), **2014**,**30**(6):1234-1242

[9] Cao X Y, Li Z J, Zhang J, et al. *CrystEngComm*, **2008**,**10**: 1345-1349

[10]Han L, Zhou Y, Zhao W N, et al. *Cryst. Growth Des.*, **2009**, **9**:660-662

[11]Li Z Z, Du L, Zhang X Z, et al. *Inorg. Chem. Commun.*, **2014**,**45**:20-24

[12]Yuan G Z, Zhu C F, Liu Y, et al. *J. Am. Chem. Soc.*, **2009**, **131**:10452-10460

[13]Huang F P, Li H Y, Tian J L, et al. *Cryst. Growth Des.*, **2009**,**9**:3191-3196

[14]Zhang J, Chen Y B, Chen S M, et al. *Inorg. Chem.*, **2006**,**45**: 3161-3163

[15]Luan X J, Cai X H, Wang Y Y, et al. *Chem. Eur. J.*, **2006**,**12**: 6281-6289

[16]Sun X L, Wang Z J, Zang S Q, et al. *Cryst. Growth Des.*, **2012**,**12**:4431-4440

[17]Cui Z H, Wang S S, Wang X G, et al. *Z. Anorg. Allg. Chem.*, **2012**,**638**:669-674

[18]Wang S S, Xi P M, Wang X G, et al. *Transition Met. Chem.*, **2013**,**38**:105-112

[19]Larsen S, Michelsen K, Pedersen E. *Acta Chem. Scand. Ser. A*, **1986**,**40**:63-76

[20]Sheldrick G M. *SADABS* 2.05, University of Göttingen, Germany, **2000**.

[21]Sheldrick G M. *Acta Crystallogr. Sect. A*, **2008**,**64**:112-122

[22]CUI Zhi-Hua(崔志华), WANG Si-Si(王思思), WANG Xiu-Guang(王修光), et al. *Chinese J. Struct. Chem.*(结构化学), **2012**,**31**(6):769-776